Volume 54
Number 17
7 May 2025
Pages 6703-7132

Dalton Transactions

An international journal of inorganic chemistry

rsc.li/dalton

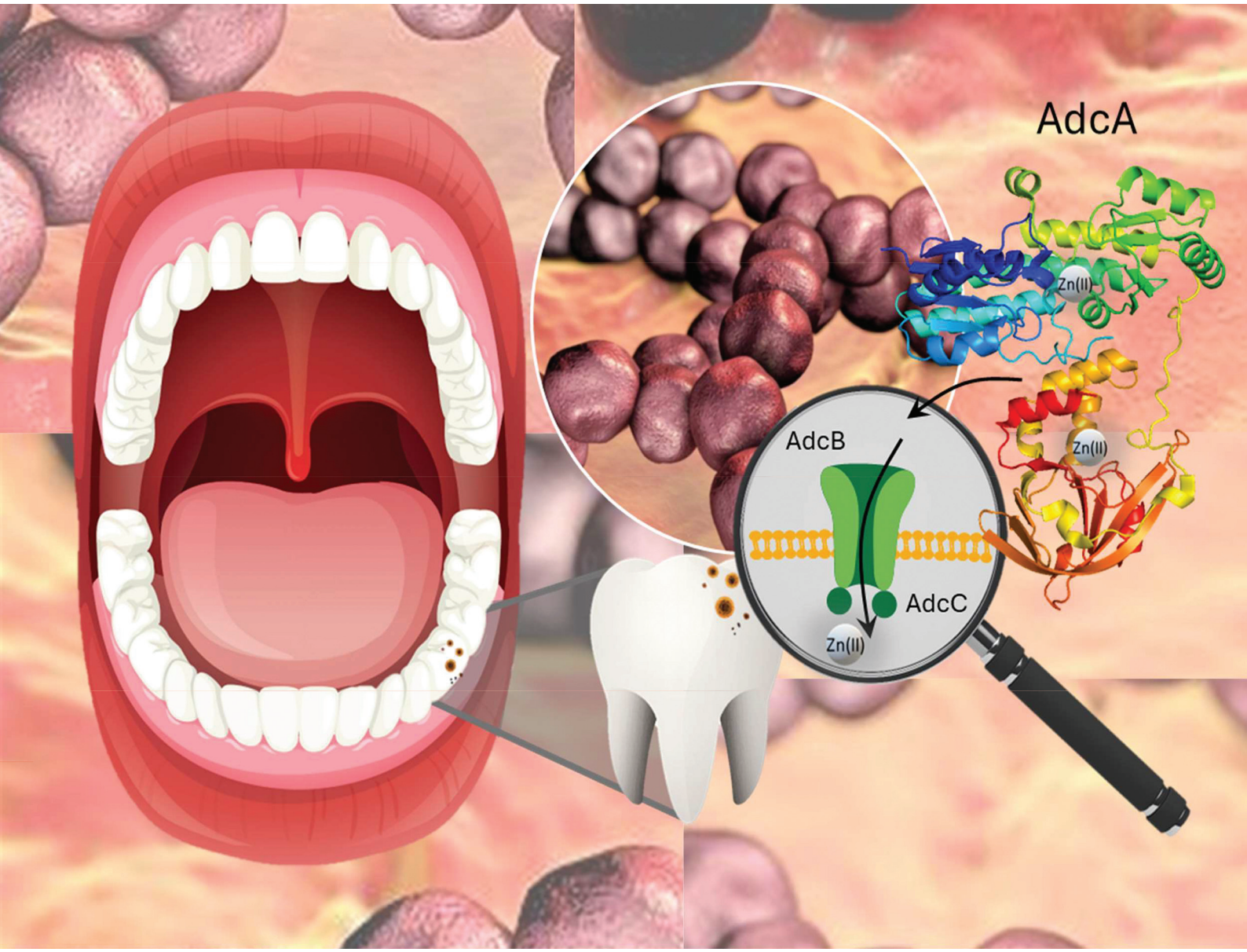

ISSN 1477-9226

ROYAL SOCIETY OF CHEMISTRY

PAPER

Aleksandra Hecel, Magdalena Rowińska-Żyrek *et al.*
AdcA lipoprotein involved in Zn(II) transport in *Streptococcus mutans* – is it as metal-specific as expected?

Dalton Transactions

ROYAL SOCIETY OF CHEMISTRY

PAPER

View Article Online
View Journal | View Issue

Cite this: *Dalton Trans.*, 2025, **54**, 6795

AdcA lipoprotein involved in Zn(II) transport in *Streptococcus mutans* – is it as metal-specific as expected?†

Kinga Garstka,[a] Aleksandra Hecel,*[a] Henryk Kozłowski,[a,b] Alicia Dominguez-Martin,[c] Krzysztof Szewczyk[d] and Magdalena Rowińska-Żyrek *[a]

Streptococcus mutans, a Gram-positive pathogen, is a primary causative agent of dental caries. It modifies the oral biofilm architecture on tooth enamel and, like other bacteria, requires transition metal ions such as Zn(II), Cu(II), and Ni(II) for survival and virulence. Physiological salivary Zn(II) levels are insufficient for optimal bacterial growth, prompting *S. mutans* to develop a specialized ABC transport system comprising AdcA, AdcB, and AdcC. Among these, the lipoprotein AdcA plays a pivotal role in Zn(II) acquisition. In this study, we examined two probable Zn(II)-binding sites in AdcA—EGHGHKGHHHA and HGIKSQKAEHFH—and their Zn(II), Cu(II), and Ni(II) complexes, keeping in mind that Cu(II) and Ni(II) are essential nutrients for bacterial enzymes and can compete with Zn(II) for its binding sites. At physiological pH, in the Zn(II)–Ac–EGHGHKGHHHA–NH_2 species, Zn(II) binds to histidine residues, forming complexes with up to four coordinated imidazole nitrogens, while in the Zn(II)–Ac–HGIKSQKAEHFH–NH_2 complex, we found three coordinated histidine side chains. The same regions of the AdcA lipoprotein are able to bind Cu(II) with even higher affinity. The stability of Zn(II) and Ni(II) complexes, on the other hand, is more comparable, with a slight advantage for Ni(II). In this case, at pH 7.4, the coordination spheres of both Zn(II) and Ni(II) consist of the same set of donor atoms. The metal binding preferences align with the Irving–Williams series; however, given the significantly higher Zn(II) concentrations in saliva and dental plaques, Zn(II) occupies the AdcA binding sites *in vivo*, highlighting its critical role in *S. mutans* virulence and metal ion homeostasis.

Received 16th January 2025,
Accepted 2nd March 2025

DOI: 10.1039/d5dt00131e

rsc.li/dalton

Introduction

Streptococcus mutans is a Gram-positive, key pathogen of dental caries,[1,2] capable of modifying the architecture of the oral biofilm formed on hard surfaces of the tooth and environment.[3,4] *S. mutans* does not act alone to cause dental caries but interacts with other organisms to assemble a cariogenic biofilm in the presence of a sugar-rich diet,[3] which changes the microenvironment for other acidogenic and aciduric bacteria, making it easier for them to establish themselves.[4] *S. mutans* causes infective endocarditis, responsible for life-threatening infection of heart valves[5] and is strongly associated with sclerosis multiplex (MS), especially in early childhood caries.[6] During its colonization, *S. mutans* has to respond and adapt to changes in the environment, like for example, oxidative and acid stress tolerance, carbohydrate utilization or the maintenance of intracellular metal ion homeostasis.[7] Its neutral habitat is human saliva – a unique body fluid, critical for oral health, due to its organic and inorganic components,[8,9] such as, among others, the divalent zinc ion.[10]

Under physiological conditions, Zn(II) is an essential element for both eukaryotic and prokaryotic cells, functioning as a structural or catalytic component of numerous proteins.[11] It is estimated that Zn(II) is present in up to 10% of all proteins in humans,[12] while in bacteria, it is found in about 5–6% of them[13] (mostly due to the smaller number of zinc finger transcription factors). Like in the case of other transition metal ions, the excess of Zn(II) might cause growth arrest and defects in the virulence of microorganisms.[7] For this reason, the intercellular concentration of bacterial Zn(II) should be strictly regulated for their survival and virulence in the human oral

[a]*Faculty of Chemistry, University of Wrocław, F. Joliot-Curie 14, 50-383 Wrocław, Poland. E-mail: magdalena.rowinska-zyrek@uwr.edu.pl, aleksandra.hecel2@uwr.edu.pl*
[b]*Institute of Health Sciences, University of Opole, Katowicka 68 St, 45-060 Opole, Poland*
[c]*Department of Inorganic Chemistry, Faculty of Pharmacy, University of Granada, E-18071 Granada, Spain*
[d]*Department of Oncology, Wrocław Medical University, pl. L. Hirszfelda 12, 53-413 Wrocław, Poland*

† Electronic supplementary information (ESI) available. See DOI: https://doi.org/10.1039/d5dt00131e

cavity.[14–17] Zn(II) is critical to the infection process, while the physiological salivary level of Zn(II) fluctuates. Below pH 6.0, most free zinc present in saliva is in the Zn(II) form, but the increase of pH drastically reduces its availability.[18] The salivary Zn(II) level also fluctuates throughout the day – between meals, the zinc concentration is limited, whereas during mealtime, its concentration increases.[7] Zn(II) is also present in the tooth enamel surface and in the dental plaque, where its concentration is much higher, reaching millimolar levels.[19] There are many different types of metal transport systems, and several of them are involved in Zn(II) homeostasis in streptococci[20] (discussed in Fig. 1).

Differently from other pathogenic bacteria that encode multiple Zn(II) import systems, *S. mutans* encodes a single, highly conserved and high affinity zinc ABC-type importer known as AdcABC.[21,22] ABC transporters (ATP-binding cassette transporters) consist of the following: AdcA, a zinc-binding lipoprotein that in Gram-positive bacteria is localized at the cell surface,[23] AdcB – a membrane permease and AdcC – a cytoplasmic ATPase[22,24–26] (adenosine 5′-triphosphatase), and their genes are regulated in response to environmental zinc availability by an adhesin competence repressor, AdcR.[27] Moreover, *S. mutans* encodes a ZccE protein, which is a P-type ATPase, responsible for Zn(II) export.[7,21,28] Also, in contrast to most streptococcal genomes, which encode two copies of adcA (called adcA and adcAII), the genome of *S. mutans* encodes a single adcA gene,[22] whose size is more similar to adcBC than to adcAII.[21] The streptococcal adcAII is genetically coupled to the pht genes (metal-binding poly-histidine triad genes) and is present in proteins that scavenge zinc, where it binds zinc outside the cell and then most probably shuttles it to AdcA.[29–31] Thus, the polyhistidine triad proteins (Pht) contain multiple copies of the histidine triad motif (HxxHxH, where x may stand for any amino acid).[32] Despite the fact that the AdcABC transporter is critical to the cariogenic potential of *S. mutans* and zinc is a growth-limiting factor for producing the oral biofilm, the genome of *S. mutans* lacks pht homologs[21,32] and *S. mutans* is the only *Streptococcus* species that does not express Pht proteins.[23] Thus, inactivating adcA or adcCB would inhibit the growth of *S. mutans*.[33–35]

For Zn(II) uptake, the *Streptococcus* species synthesizes the double-domain AdcA protein with two zinc-binding sites: the N-terminal and C-terminal domains (Fig. 2). The N-terminal domain, in the presence of Zn(II), quickly and strongly binds the metal and then changes its conformation, which stabilizes the second, C-terminal domain (H36, H122, H186, and E261).[36] A tight zinc-binding pocket facilitates zinc binding, and the relatively less stable binding and conformation of the C-terminal domain (H436, H445, and H447) ensure a rapid transfer of Zn(II) from AdcA to the transmembrane AdcB protein.[36] As in other streptococci, AdcA from *S. mutans* has two zinc-binding domains: the N-terminal domain, which consists of five histidine residues (H132, H134, H137, H138, and H139 – Fig. S1, ESI†), and the C-terminal domain, which contains three histidine residues in close proximity (H457, H466, H468 – Fig. S1, ESI†).[21]

Another well-conserved and potentially metal-binding site contains three conserved histidine residues (H70, H144, and H208) and one glutamic acid residue (E294).[21] This AdcA-based high-affinity Zn(II) transport system is homologous to the one from *Escherichia coli* ZnuA,[37] ZnuA and AztC solute binding proteins from *Paracoccus denitrificans*[38] or to the fungal zincophore-based transport systems, comprising proteins with high Zn(II) affinity that are synthesized in the cytoplasm and then exported to bind Zn(II).[39–42]

During infection, the host limits the availability of micronutrients for pathogens at the colonization surface in a process referred to as nutritional immunity[43–45] and plays a role in

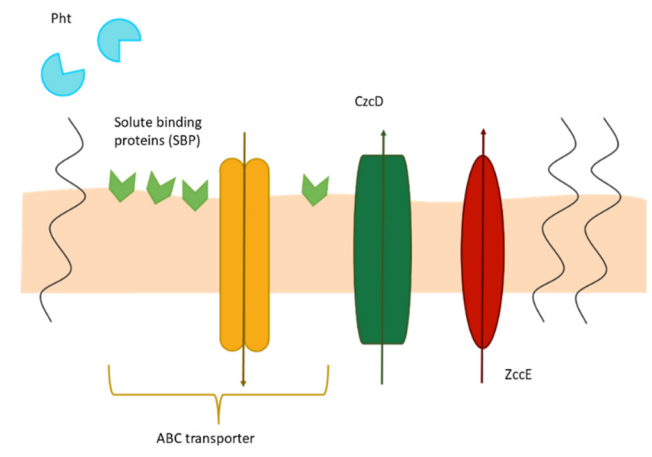

Fig. 1 A summary diagram of all known types of transporters for Zn(II) in streptococci, with arrows indicating metal import or export: histidine triad proteins (Pht), ABC transporter, CDF pump (cation diffusion facilitator): CzcD. The ZccE (P-type ATPase) is only found in *S. mutans*.

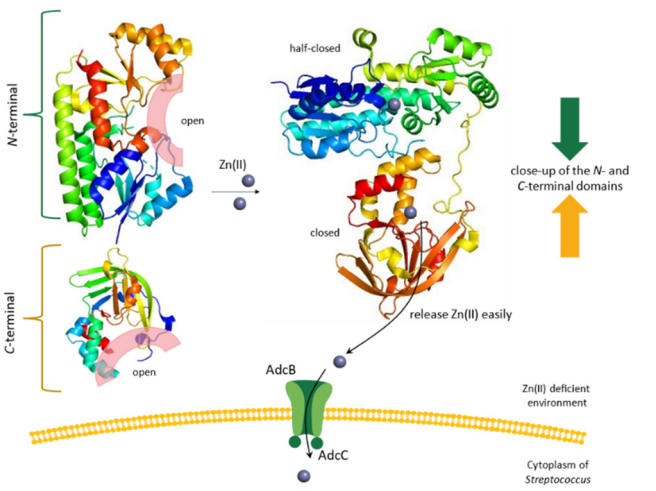

Fig. 2 The model of Zn(II) uptake in *Streptococcus via* AdcA in a Zn(II)-deficient environment. The N- and C-terminal domains of AdcA are marked green and yellow, respectively. The two binding sites are represented as an open state without metal ions (left part) and a half-closed or closed state in Zn(II)-bound AdcA (right part). The AdcA structures are based on the files from the Protein Data Bank (accession codes: 7JJ9, 7JJ8, 7JJA and 7JJB).

host defence against pathogenic microorganisms, constituting an ideal therapeutic target in times of increasing antibiotic resistance. Antimicrobial peptides are a promising direction to find new, effective, and specific drugs, and their use in STAMP technology (specifically targeted antimicrobial peptides) increases the chances of winning the fight against microorganisms. STAMP is based on two domains: an antimicrobial domain (an antimicrobial peptide – AMP, small host defence peptides that form part of the innate immune response[46]) and a targeting domain (a fragment of the protein from the pathogen), linked *via* a short flexible linker.[47] A precise understanding of the Zn(II) transport mechanism present in pathogens is an important research direction towards the design of a targeting domain for new, highly specific therapeutics against antibiotic-resistant bacterial species.

Because biofilm formation is a survival strategy by which *S. mutans*, an important factor for the initiation of dental caries, adapts to its environment, we focused on Zn(II), Cu(II) and Ni(II) complexes of two regions of the AdcA lipoprotein involved in Zn(II) transport in *Streptococcus mutans*: Ac–EGHGHKGHHHA–NH_2 and Ac–HGIKSQKAEHFH–NH_2 (highlighted in red in Fig. S1, ESI†). We checked their structural and thermodynamic properties using a number of complementary methods: potentiometry, EPR, UV-Vis and CD spectroscopy. The results allowed us to provide information on the protonation and stability constants, identify the number and types of donor atoms involved in Zn(II), Cu(II), and Ni(II) binding and determine the influence of metal ions on the secondary structure of the analyzed ligands.

Experimental

Synthesis

Peptides (Ac–EGHGHKGHHHA–NH_2 and Ac–HGIKSQKAEHFH–NH_2) were purchased from KareBay Biochem (certified purity: 98%) and were used as received. The carbonate-free stock solution of 0.1 M NaOH was purchased from Sigma-Aldrich and then potentiometrically standardized with potassium hydrogen phthalate. Zinc perchlorate, copper perchlorate and nickel chloride were extra-pure products (Sigma-Aldrich). The concentrations of salt solutions were determined by inductively coupled plasma (ICP) mass spectrometry.

Potentiometric measurements

The stability constants for Ac–EGHGHKGHHHA–NH_2 and Ac–HGIKSQKAEHFH–NH_2 ligands and their Zn(II), Cu(II) and Ni(II) complexes were calculated from titration curves carried out in the pH range of 2–11 at 298 K in 0.1 M $NaClO_4$. The total volume of the solution used was 3.0 cm^3. The potentiometric titrations were performed using a Dosimat 800 Metrohm titrator connected to a Metrohm 905 pH meter and a Mettler Toledo pH inLab Science electrode. The glass cell was equipped with a magnetic stirring system, a microbiuret delivery tube and an inlet–outlet tube for argon. Solutions were titrated with 0.1 M carbonate-free NaOH. The electrodes were calibrated daily for hydrogen ion concentration by titrating $HClO_4$ with NaOH using a total volume of 3.0 cm^3. The purities and the exact concentrations of the ligand solutions were determined using the Gran method. The ligand concentration was 0.5 mM. The Zn(II), Cu(II) and Ni(II) to ligand ratio was 0.8 : 1. The HYPERQUAD 2006 program was used for the stability constant calculations.[48] The standard deviations were computed using HYPERQUAD 2006 and referenced to random errors only. The constants for hydrolytic Zn(II) and Ni(II) species were used in these calculations.[49,50] The speciation and competition diagrams were computed using the HYSS program.[51]

Spectroscopic studies

The absorption spectra were recorded on a Jasco-730 spectrophotometer in the range 200–800 nm, using a quartz cuvette with an optical path of 1 cm. Circular dichroism spectra were recorded on a Jasco J-1500 CD spectrometer in the 250–800 nm and 180–250 nm ranges, using a quartz cuvette with an optical path of 1 cm and 0.01 cm in the visible and near-UV range. The concentration of sample solutions used for spectroscopic studies was similar to that employed in the potentiometric experiment. The metal : ligand ratio was 0.8 : 1. All spectroscopic measurements were recorded in the pH range 2.5–10.5. The pH of the samples was adjusted with appropriate amounts of concentrated $HClO_4$ and NaOH solutions. OrginPro 2016 was used to process and visualize the obtained spectra.[52] Electron paramagnetic resonance (EPR) spectra were recorded in liquid nitrogen on a Bruker ELEXSYS E500 CW-EPR spectrometer at an X-band frequency (9.5 GHz) and equipped with an ER 036TM NMR teslameter and an E41 FC frequency counter. The ligands were prepared in an aqueous solution of $HClO_4$ at I = 0.1 M ($NaClO_4$). The concentration of Cu(II) was 1 mM, and the metal : ligand ratio was 0.8 : 1. Ethylene glycol (25%) was used as a cryoprotectant for EPR measurements. The EPR parameters were analyzed by computer simulation of the experimental spectra using WIN-EPR SIMFONIA software, version 1.2 (Bruker). The pH was adjusted with appropriate amounts of $HClO_4$ and NaOH solutions.

Results

Ligand protonation

Both peptides (Ac–EGHGHKGHHHA–NH_2 and Ac–HGIKSQKAEHFH–NH_2) are protected on the N-terminus by acetylation but also on the C-terminus by amidation. The Ac–EGHGHKGHHHA–NH_2 peptide behaves as an LH_7 acid with the protonating groups corresponding to the deprotonation of the carboxylic side chain of glutamic acid (pK_a = 3.87), five histidine imidazole side chain groups (pK_a values of 5.48, 5.73, 6.47, 6.51 and 7.46, respectively) and to the deprotonation of the lysine side chain group with a pK_a value of 10.07 (Table 1). The Ac–HGIKSQKAEHFH–NH_2 peptide has six protonation constants. The first one (pK_a = 3.90) can be assigned to the deprotonation of the carboxylic side chain of glutamic acid.

Table 1 Potentiometric data for the proton, Zn(II), Cu(II) and Ni(II) complexes of Ac–EGHGHKGHHHA–NH_2 and Ac–HGIKSQKAEHFH–NH_2 in a water solution of 4 mM $HClO_4$ with I = 0.1 M $NaClO_4$, T = 298 K. Standard deviations are presented in parentheses

	Ac–EGHGHKGHHHA–NH_2			Ac–HGIKSQKAEHFH–NH_2		
Species	Log β	Log K	Residue	Log β	Log K	Residue
HL	10.07(1)	10.07	(K)	10.56(1)	10.56	(K)
H_2L	17.54(3)	7.46	(H)	20.43(1)	9.88	(K)
H_3L	24.05(3)	6.51	(H)	27.51(1)	7.08	(H)
H_4L	30.52(3)	6.47	(H)	33.86(1)	6.35	(H)
H_5L	36.25(3)	5.73	(H)	39.71(2)	5.84	(H)
H_6L	41.72(3)	5.48	(H)	43.60(2)	3.90	(E)
H_7L	45.59(3)	3.87	(E)			
Zn(II) complexes						
ZnH_3L	29.00(1)			30.88(1)		
ZnH_2L	22.85(1)	6.14	(H)	25.13(1)	5.75	(H)
ZnHL	15.92(2)	6.93	(H)	17.37(2)	7.76	(H_2O)
ZnL	7.46(2)	8.46	(H_2O)	9.24(2)	8.13	(H_2O)
$ZnH_{-1}L$	−2.11(3)	9.58	(K)	−0.60(3)	9.84	(K)
$ZnH_{-2}L$				−11.19(4)	10.51	(K)
Cu(II) complexes						
CuH_4L	36.62(1)					
CuH_3L	32.28(1)	4.34	(H)	33.73(3)		
CuH_2L	26.91(2)	5.37	(H)	28.18(5)	5.55	(H)
CuHL	20.35(2)	6.56	(am)	22.49(4)	5.69	(am)
CuL	12.69(3)	7.66	(am)	15.68(5)	6.81	(am)
$CuH_{-1}L$	5.23(3)	7.46	(am)	8.24(4)	7.44	(am)
$CuH_{-2}L$	−4.40(5)	9.63	(K)	−1.00(7)	9.24	(K)
$CuH_{-3}L$				−10.60(5)	9.60	(K)
Ni(II) complexes						
NiH_4L				36.56(8)		
NiH_3L	29.02(1)			31.45(1)	5.11	(H)
NiH_2L	22.87(1)	6.15	(H)	25.48(1)	5.98	(H)
NiHL	16.00(1)	6.87	(H)			
NiL	7.61(2)	8.39	(am)	8.61(1)		
$NiH_{-1}L$	−1.90(2)	9.51	(am)	−0.78(1)	9.38	(am)
$NiH_{-2}L$				−11.04(1)	10.27	(K)
$NiH_{-3}L$	−23.65(4)		(K)	−21.59(1)	10.55	(K)

The next three constants (pK_a = 5.84, 6.35 and 7.08) are related to the deprotonation of three histidine imidazole groups and the last two (pK_a = 9.88 and 10.56) correspond to the deprotonation of two lysine side chain groups (Table 1).

Metal complexes of Ac–EGHGHKGHHHA–NH_2

Zn(II) complexes. The first Zn(II)–Ac–EGHGHKGHHHA–NH_2 complex form, ZnH_3L, has its maximum at pH 5.8 (Fig. S2A, ESI†). It involves one glutamic acid residue and two histidine residues in binding. The loss of one proton leads to the ZnH_2L form, which dominates in the solution of around pH 6.5 and is most probably related to the deprotonation of the non-coordinating histidine residue (due to no significant changes in the pK_a values of 6.51 and 6.14 for the free and complexed one, respectively) (Table 1). The next form, ZnHL, has a maximum at pH 7.7 and is most likely related to the deprotonation and coordination of the next imidazole nitrogen of the histidine residue. Loss of the next proton leads to the formation of the ZnL form, related to the proton loss of a water molecule bound to the Zn(II) atom. The last form, $ZnH_{-1}L$, is connected with the deprotonation of a non-coordinating lysine residue.

Cu(II) complexes. The stability constants for Cu(II) complexes with Ac–EGHGHKGHHHA–NH_2 were calculated on the basis of the titration curves recorded in the pH range of 2.0–11.0. Potentiometric measurements revealed the presence of seven equimolar complex species (Fig. S3A, ESI†). In the first species detected at low pH, CuH_4L, with a maximum concentration at pH 4.4 (Fig. S3A, ESI†), characteristic bands in the UV-Vis and CD spectra (λ_{max} = 640 nm with ε = 54.81 (Fig. S4A, ESI†) and λ_{max} = 256 nm with $\Delta\varepsilon$ = 0.64 (Fig. S5A, ESI†)) can be assigned to the coordination of Cu(II) by one or a maximum of two histidyl residues (Table S1, ESI†). The next CuH_3L species results from the coordination of two histidyl residues. The coordination of Cu(II) to two imidazole nitrogens is supported by the d–d band at 627 nm and EPR parameters A_{II} = 171; g_{II} = 2.28 at pH 5.0 (Fig. S6A, ESI†). The shift of the d–d band from 627 to 606 nm suggests the coordination of a third imidazole nitrogen for the CuH_2L with the maximum concentration at 6.0 (EPR parameters A_{II} = 188; g_{II} = 2.25). Moreover, the significant lowering of pK_a values in Cu(II) complexes compared to free ligands is observed (pK_a 5.37 and 6.51, respectively). The presence of one negative band at around 550 nm for CuH_4L, CuH_3L and CuH_2L species may suggest additional coordi-

nation of the carboxyl group of the glutamic acid. The coordination of an amide nitrogen atom occurs at pH above 6.5, as evidenced by the appearance of intense d–d bands in CD spectra (λ_{max} = 545 nm with ε = −0.22 and λ_{max} = 643 nm with ε = 0.11) for CuHL species (Fig. S5A, ESI†). The $\{2N_{im}, 1N^-\}$ complex for CuHL is confirmed by the d–d band at 604 nm and EPR parameters A_{II} = 195 and g_{II} = 2.23. The increase of signal intensity observed in the CD and UV–Vis spectra supports coordination with further amide nitrogen atoms above pH 7.5, while not changing the number of nitrogen atoms in the 3N coordination sphere. The coordination mode for CuHL is $\{1N_{im}, 2N^-\}$. At pH above 8.5, the intensity of the d–d bands increases, and the differences in the d–d transition energy (*i.e.*, a shift of the band to shorter wavelengths λ_{max} = 571 nm) indicate the coordination of the third amide nitrogen, forming a square-planar $\{N_{im}, 3N^-\}$ complex for $CuH_{-1}L$ species. The last form, $CuH_{-2}L$, results from the deprotonation of a non-coordinating lysine residue (pK_a = 9.63). The 4N coordination for the last two species is supported by the EPR parameters A_{II} = 205 and g_{II} = 2.21.

Ni(II) complexes. For Ac–EGHGHKGHHHA–NH_2, we observe six complex forms with Ni(II) ions (Fig. S7A, ESI†). The first one is NiH_3L with a maximum at pH 5.7. Most probably, it engages three histidine residues in binding. The increase of pH leads to the NiH_2L form, which corresponds to the deprotonation of the subsequent histidine residue, which does not participate in binding (the low pK_a difference for this group between the free ligand (6.57) and the complexed one (6.15) confirms this theory). In this pH, the coordination mode does not change. The next form, NiHL, dominates in the solution above pH 6.9. The lowered pK_a value (7.46 and 6.87 for the free ligand and the complexed one, respectively) indicates the deprotonation and engagement of the last available histidine residue in Ni(II) binding. The following NiL and $NiH_{-1}L$ forms, with maxima at around pH 8.9 and 10.2, respectively, are connected with the deprotonation and binding of two amide nitrogen atoms. Therefore, the Ni(II) coordination sphere includes two histidine imidazole groups and two amide nitrogen atoms. Around pH 8, a CD band (Fig. S8A, ESI†), which appears near 415.9 nm (a positive Cotton effect) and 497.2 nm (a negative Cotton effect) can be assigned to the $N^- \rightarrow Ni(II)$ transition[53] and confirms this finding (in the pH range from 8.0 to 11.0, the intensity of the bands increases). The involvement of two amide nitrogen atoms in binding is also confirmed by UV-Vis spectroscopy (Fig. S9A, ESI†), where from pH 9.0, a band with a maximum at around 438.4 nm is observed. At a very basic pH value, the $NiH_{-3}L$ complex is detected, and it can be assigned to the deprotonation of the lysine residue, which most probably does not participate in binding.

Metal complexes of Ac–HGIKSQKAEHFH–NH_2

Zn(II) complexes. The first acidic Zn(II)–Ac–HGIKSQKAEHFH–NH_2 complex is ZnH_3L, with a maximum at pH 6.0 (Fig. S2B, ESI†) and most probably involves two imidazole groups in coordination. The next form, ZnH_2L, with a maximum at pH 7.0 is related to the proton loss and coordination of the next histidine residue. A significant decrease of the pK_a values calculated for the complexes (pK_a = 5.75) and free imidazole (pK_a = 7.08) suggests that the histidine residue is involved in Zn(II) binding (Table 1). The next two observed forms, ZnHL and ZnL, correspond to the deprotonation of two water molecules and the remaining two deprotonations are most likely related to the proton loss of two non-coordinating lysine residues.

Cu(II) complexes. Cu(II)–Ac–HGIKSQKAEHFH–NH_2 shows seven complex forms (Fig. S3B, ESI†). The first acidic form (CuH_3L) achieves its maximum at a pH of around 4.9. The absorption spectrum (λ_{max} = 672 nm) and EPR parameters (A_{II} = 152, g_{II} = 2.31) at pH 5.0 suggest the coordination of one or two nitrogen atoms (Fig. S6B, ESI, Table S2, ESI†). The next complex, CuH_2L, is likely characterized by a $\{3N_{im}\}$ coordination. An increasing UV–Vis band at 619 nm and EPR parameters A_{II} = 170 and g_{II} = 2.26 confirm the 3N coordination at pH 5.6. A comparison between the pK_a values of the free ligand and the complexed one (7.08 and 5.55, respectively) strongly suggests that a third histidine imidazole is also involved in Cu(II) binding. The Cu(II) interaction with the backbone amides likely begins at around pH 6. This is highlighted by the circular dichroism spectra (Fig. S5B, ESI†), where the increase in the CD positive and negative signal intensity (λ_{max} = 544 nm with ε = −0.51 and λ_{max} = 635 nm with ε = 0.33) can be ascribed to the formation of a square-planar $\{3N_{im}, 1N^-\}$ complex for CuHL species (max concentration at pH 6.3). Moreover, EPR parameters, A_{II} = 193 and g_{II} = 2.20, prove 4N complex formation (Fig. S6B, ESI†). Moving to alkaline conditions, we observed the formation of $\{2N_{im}, 2N^-\}$ and $\{1N_{im}, 3N^-\}$ complexes for CuL and $CuH_{-1}L$ species, respectively. The lack of significant differences in the absorption spectra for the last two forms, $CuH_{-2}L$ and $CuH_{-3}L$, still provides 4N complexes with the deprotonation of two lysine residues (pK_a 9.24 and 9.60), which do not participate in coordination.

Ni(II) complexes. In the case of Ac–HGIKSQKAEHFH–NH_2, Ni(II) coordination starts at pH 4.0 and the first observed form is NiH_4L with a maximum at pH 5.5 (Fig. S7B, ESI†). Most probably, it involves one histidine residue in binding. The next two forms, NiH_3L and NiH_2L, with maxima at pH 6.0 and 7.4, respectively, are both related to the proton loss and coordination of histidine residues. A significant decrease of the pK_a values calculated for the complexed and free imidazole (pK_a = 5.11 and 6.35; pK_a = 5.98 and 7.08, respectively) suggests that both residues are involved in Ni(II) binding. Above pH 8.5, the NiL form dominates in solution. Around this pH, a CD band at 260.0 nm, which can be related to the $N^- \rightarrow Ni(II)$ charge transfer transitions[53] is observed (Fig. S7B, ESI†). The increase of pH leads to the $NiH_{-1}L$ form, in which most probably the Ni(II) coordination sphere includes two histidine imidazole groups and two amide nitrogen atoms – the CD band with the negative Cotton effect at 425.0 nm and the positive Cotton effect at 525.0 nm and the UV-Vis band at 420.0 nm confirm this finding and can be assigned to the square planar nickel complex (Fig. S8B, ESI†). The last two forms, $NiH_{-2}L$ and $NiH_{-3}L$, correspond to the deprotonation of two lysine residues, which do not participate in coordination.

Secondary structure

The coordination of Zn(II) and Cu(II) influences pronounced secondary structural changes of both Ac–EGHGHKGHHHA–NH_2 and Ac–HGIKSQKAEHFH–NH_2 AdcA regions (Fig. 3). At pH 7.4, both peptides are random coils, with a positive absorption band around 215 nm and a negative one below 200 nm.[54] Metal coordination changes the CD spectra and therefore also the secondary structure of the complexed ligands – for both Zn(II) and Cu(II) complexes, the intensity of the spectral minima becomes smaller and the minima and maxima shift to *ca.* 195 nm and 210 nm, respectively. Although these parameters are not typical for any particular structure (they are sometimes inadequately assigned to PPII like helices in the literature), it is clear that metal coordination significantly induces structural changes.

Ni(II) coordination is an interesting case – its binding appears to have almost no structural impact on the overall structure of Ac–HGIKSQKAEHFH–NH_2, while in the case of Ac–EGHGHKGHHHA–NH_2, it induces a significant structural rearrangement, enhancing and shifting the CD maximum at 215 nm and making the spectral minimum at 195 nm much more shallow.

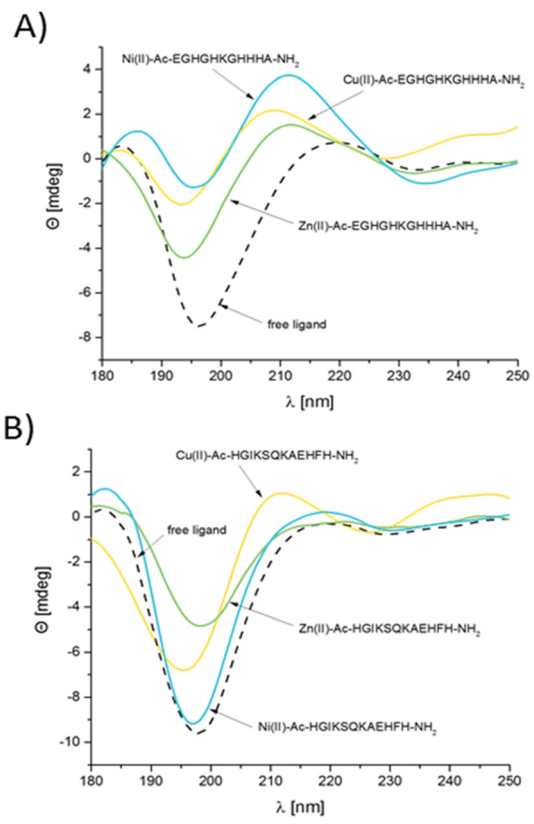

Fig. 3 Far UV CD spectra of the (A) Ac–EGHGHKGHHHA–NH_2 and (B) Ac–HGIKSQKAEHFH–NH_2 fragments with Zn(II), Cu(II) and Ni(II) in the range of 180–250 nm, pH 7.4, T = 298 K; optical path = 0.01 cm; [L] = 0.0005 M; M(II)/L = 0.8 : 1.

Discussion

Is it theoretically possible for other biologically relevant metal ions, Cu(II) and Ni(II), necessary for proper growth and replication of microorganisms, to compete with Zn(II) for the binding sites in the AdcA protein?

In order to identify the AdcA fragment that binds Zn(II), Cu(II) and Ni(II) with the highest affinity, we used the thermodynamic data for the metal complexes to simulate a theoretical situation in which equimolar amounts of Zn(II) and both studied unstructured AdcA fragments were mixed. This allows a direct comparison of the calculated constants at different pH

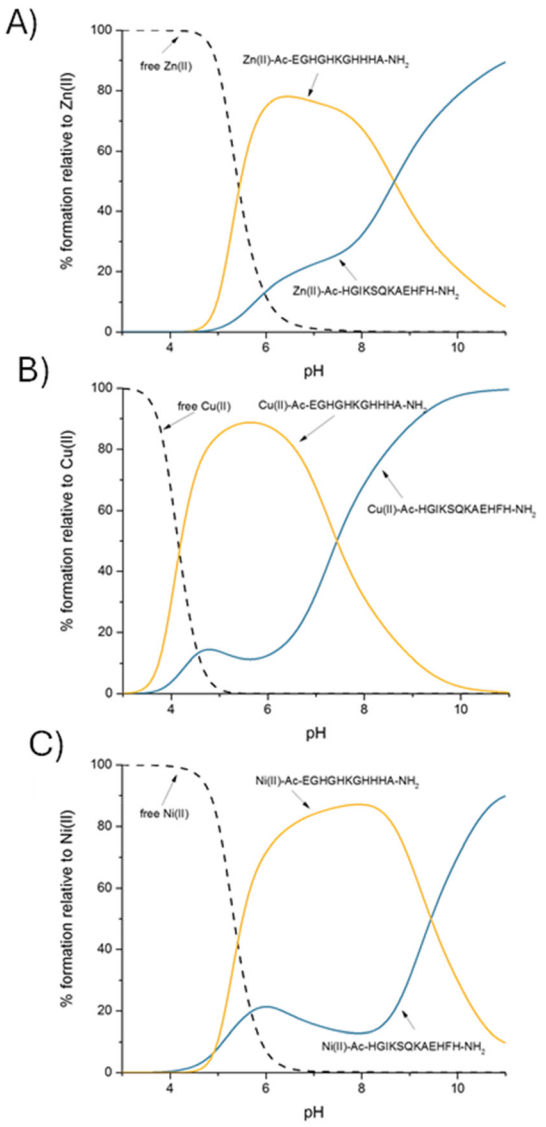

Fig. 4 A competition plot between AdcA fragments: Ac–EGHGHKGHHHA–NH_2 and Ac–HGIKSQKAEHFH–NH_2 and (A) Zn(II), (B) Cu(II) and (C) Ni(II), describing complex formation at different pH values in a hypothetical situation in which equimolar amounts of all reagents are mixed. Calculations are based on binding constants from Table 1. Conditions: T = 298 K, I = 0.1 M $NaClO_4$, [Ac–EGHGHKGHHHA–NH_2]=[Ac–HGIKSQKAEHFH–NH_2]=[Zn(II)]=[Cu(II)]=[Ni(II)] = 0.001 M.

values (Fig. 4A) and shows that in almost the entire pH range, the Ac–EGHGHKGHHHA–NH_2 ligand is preferred over the Ac–HGIKSQKAEHFH–NH_2 one, which is not surprising, since the Ac–EGHGHKGHHHA–NH_2 region contains more histidine residues (five *vs.* three in the Ac–HGIKSQKAEHFH–NH_2 ligand). At pH 7.4, more than 70% of available Zn(II) would be bound to Ac–EGHGHKGHHHA–NH_2.

A very interesting case is observed for Cu(II) complexes with the studied ligands; at acidic pH, Cu(II) prefers to bind to the more His-rich Ac–EGHGHKGHHHA–NH_2 region, while at basic pH, in which amide nitrogens dominate in the Cu(II) coordination sphere, the Ac–HGIKSQKAEHFH–NH_2 fragment is preferred. Interestingly, at pH 7.4, the two complexes are almost equally stable (Fig. 4B). Ni(II) also chooses Ac–EGHGHKGHHHA–NH_2 over Ac–HGIKSQKAEHFH–NH_2 almost in the entire pH range, in which His imidazoles are the metal binding sites; at pH 7.4, in our hypothetical situation, more than 85% of the metal would be bound to the His-rich Ac–EGHGHKGHHHA–NH_2 region. As in the case of Cu(II), the situation changes dramatically in an alkaline environment when amide nitrogens are involved in coordination – the Ni(II)–Ac–HGIKSQKAEHFH–NH_2 complex becomes more stable (Fig. 4C). To summarize, poly-His complexes are more tempting metal binding sites at lower pH values, while at higher pH, when amide nitrogens are involved in Cu(II) and Ni(II) coordination, the affinity of poly-His sites turns out to be lower than that of the sequence with a lower number of His residues, which is more likely to involve an amide in binding.

The Ac–EGHGHKGHHHA–NH_2 region itself strongly prefers Cu(II) over Zn(II) and Ni(II), which is consistent with the Irving–Williams series.[55,56] Even in a theoretical situation in which equimolar amounts of Zn(II), Cu(II) and Ni(II) would be available, in the whole pH range, the sequence strongly prefers to bind Cu(II) (Fig. 5A). As far as Zn(II) and Ni(II) binding preferences are concerned, up to pH 7.4, no significant differences

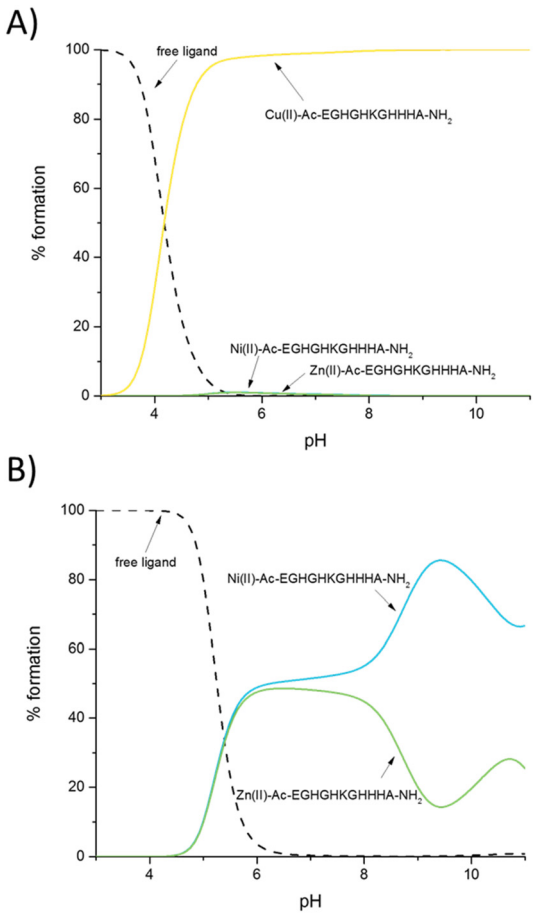

Fig. 5 A competition plot between (A) the AdcA fragment: Ac–EGHGHKGHHHA–NH_2, Zn(II), Cu(II) and Ni(II) and (B) the AdcA fragment: Ac–EGHGHKGHHHA–NH_2, Zn(II), and Ni(II), describing complex formation at different pH values in a hypothetical situation in which equimolar amounts of all reagents are mixed. Calculations are based on binding constants from Table 1. Conditions: T = 298 K, I = 0.1 M $NaClO_4$, (A) [Ac–EGHGHKGHHHA–NH_2]=[Zn(II)]=[Cu(II)]=[Ni(II)] = 0.001 M; (B) [Ac–EGHGHKGHHHA–NH_2]=[Zn(II)]=[Ni(II)] = 0.001 M.

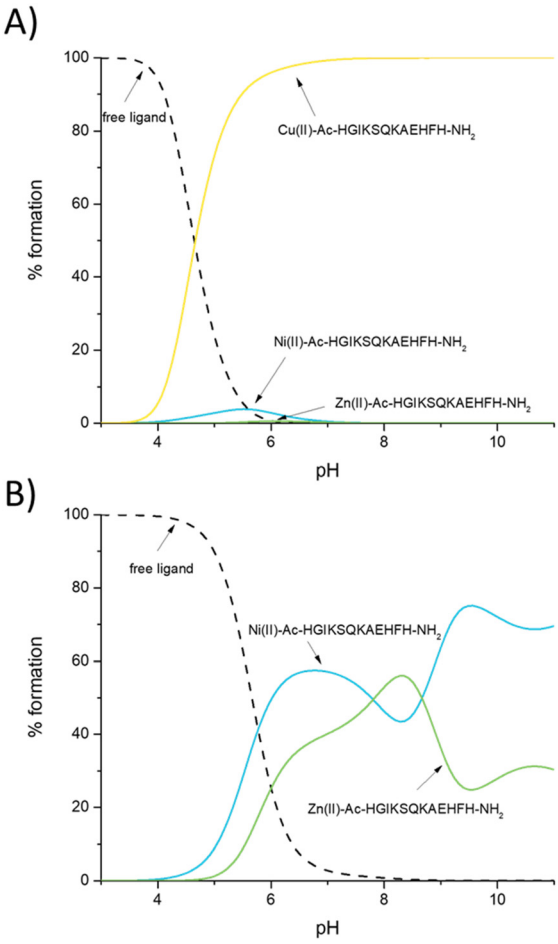

Fig. 6 A competition plot between (A) the AdcA fragment: Ac–HGIKSQKAEHFH–NH_2, Zn(II), Cu(II) and Ni(II) and (B) the AdcA fragment: Ac–HGIKSQKAEHFH–NH_2, Zn(II), and Ni(II), describing complex formation at different pH values in a hypothetical situation in which equimolar amounts of all reagents are mixed. Calculations are based on binding constants from Table 1. Conditions: T = 298 K, I = 0.1 M $NaClO_4$, (A) [Ac–HGIKSQKAEHFH–NH_2]=[Zn(II)]=[Cu(II)]=[Ni(II)] = 0.001 M; (B) [Ac–HGIKSQKAEHFH–NH_2]=[Zn(II)]=[Ni(II)] = 0.001 M.

in the stability of both complexes are observed – the two metals bind with almost identical affinity, which is quite surprising. The situation changes in an alkaline environment when amide nitrogens are involved in the coordination of Ni(II), and the Ni(II)–Ac–EGHGHKGHHHA–NH_2 complex becomes significantly more stable than the Zn(II) one (Fig. 5B).

A very analogous situation is observed for Ac–HGIKSQKAEHFH–NH_2: consistent with the Irving–Williams series,[55,56] the Cu(II)–Ac–HGIKSQKAEHFH–NH_2 complex is the most stable one (Fig. 6A). As for the Zn(II) and Ni(II) specificity of this region, it seems to have no strong metal preference up to pH 9. At basic pH, the coordination of amide nitrogens in Ni(II) complexes gives them greater stability than Zn(II) complexes (Fig. 6B), as in the case of the previous ligand (Fig. 5B).

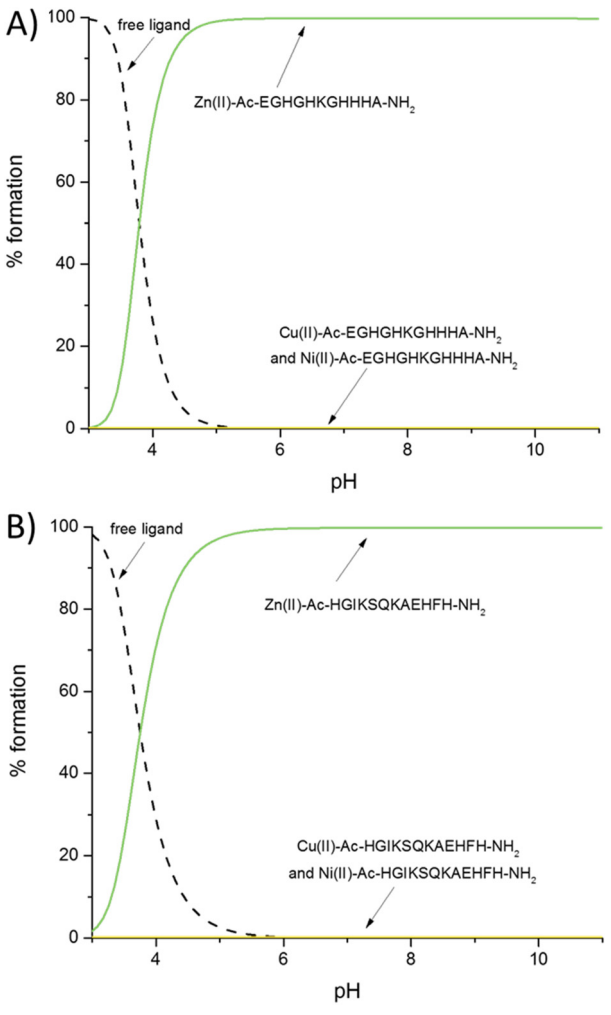

Fig. 7 A competition plot between (A) Ac–EGHGHKGHHHA–NH_2, Zn(II), Cu(II) and Ni(II) and (B) Ac–HGIKSQKAEHFH–NH_2, Zn(II), Cu(II) and Ni(II), describing complex formation at different pH values in a hypothetical situation in which appropriate amounts of all reagents are mixed. Calculations are based on binding constants from Table 1; hypothetical metal concentrations are taken from the literature.[19,57,58] Conditions: T = 298 K, I = 0.1 M $NaClO_4$, (A) [Ac–EGHGHKGHHHA–NH_2]=[Zn(II)] = 0.001 M; (B) [Ac–HGIKSQKAEHFH–NH_2]=[Zn(II)] = 0.001 M.

Metal ions like Zn(II), Cu(II) and Ni(II) are found naturally in saliva, teeth and dental plaques and to compare the stability of Zn(II), Cu(II), and Ni(II) complexes with those naturally found in the human body, we simulated a hypothetical situation in which the studied sequences Ac–EGHGHKGHHHA–NH_2, Ac–HGIKSQKAEHFH–NH_2 and metals were mixed in appropriate concentrations in which the metal ions could be found in the oral cavity (Fig. 7). Their concentrations are quite variable and depend on the diet, occupational exposure, salivary flow rate, exposure to toxic metals, disease states or quantity of metal-binding proteins. However, the Zn(II) concentration in saliva is within the range of 0.01–0.25 μg ml^{-1}.[19] In dental plaques, the Zn(II) concentration is higher and fluctuates from 6 to 20 μg ml^{-1}, while the Cu(II) concentration on the enamel surface is much lower, 0.037 μg ml^{-1}.[57] The concentration of Ni(II) in saliva has also been tested and varies between numbers as low as 0.001 and 0.0019 μg ml^{-1}, but may even reach 0.19 μg ml^{-1} in the case of orthodontic treatment.[58]

The results clearly indicate that in a physiological environment, both ligands (Ac–EGHGHKGHHHA–NH_2 (Fig. 7A) and Ac–HGIKSQKAEHFH–NH_2 (Fig. 7B)) will be found bound to Zn(II) rather than to Cu(II) or Ni(II). The saliva and dental plaque Zn(II) concentrations are much higher than those of Cu(II) and Ni(II); thus, the trend is constant over the entire pH range. This guarantees an efficient Zn(II) transport in *S. mutans* using the AdcA protein, despite the affinities towards Ni(II) being quite high for both studied regions.

Conclusions

In response to nutritional resistance, bacteria have evolved mechanisms to acquire essential metal ions. One key strategy to mitigate Zn(II) deficiency is the use of ABC transporters. In this study, we identified two likely binding sites in the AdcA lipoprotein of *Streptococcus mutans*, a bacterial pathogen associated with dental caries. A detailed understanding of this Zn(II) transport mechanism in *S. mutans* represents a significant step toward elucidating metal transport systems in other pathogens and designing targeted therapeutics against antibiotic-resistant bacterial species.

At physiological pH, the Ac–EGHGHKGHHHA–NH_2 region binds Zn(II) with higher affinity than the Ac–HGIKSQKAEHFH–NH_2 one. The binding preferences of Cu(II) and Ni(II), metal ions that could potentially compete with Zn(II) binding to AdcA, involve not only histidine imidazoles but also amide nitrogen atoms. Despite differences in coordination modes, it seems interesting that almost all metal ions have an influence on the secondary structures of both studied ligands, leading to pronounced changes in their random coil structures. In accordance with the Irving–Williams series, the Cu(II)–AdcA complexes are most stable (compared to Zn(II) and Ni(II) ones; at pH 7.4, at equimolar concentrations, more than 98% of analyzed sequences would bind Cu(II)), while the stability of Zn(II) and Ni(II) complexes is comparable. Given the high Zn(II) concentrations in human saliva and dental plaques, Zn(II)–AdcA

complexes are expected to dominate in the oral cavity, rendering Cu(II) and Ni(II) binding affinities less relevant under physiological conditions.

These findings provide valuable insights into the chemistry of Zn(II), Cu(II), and Ni(II), as well as metal transport mechanisms in pathogens. Importantly, they underscore the necessity of considering physiological metal ion concentrations when evaluating competition for biologically relevant ligands. In essence, "high affinity is not enough; high concentration is far more significant".

Understanding the metal binding specificity of AdcA paves the way for designing specific AdcA inhibitors that selectively reduce *S. mutans* growth. Several key factors must be considered in this process – the inhibitor must specifically target the AdcA protein in *S. mutans*, while avoiding disruption of proteins beneficial for the host. Such an inhibitor should block the interaction between AdcA and metals, which would prevent zinc uptake, disrupting the bacterium's zinc homeostasis and leading to its death. Inhibitors could also interfere with the interaction between AdcA and other components of the AdcABC system, such as AdcB and AdcC, potentially inhibiting the entire zinc transport process. Another approach may be effective in the fight against antibiotic resistance: using AdcA as a targeting molecule in the STAMP (specifically targeted antimicrobial peptide) method[59] that could involve attaching an antibiotic or antimicrobial peptide to an AdcA peptide fragment that is selectively recognized by its partner on the bacterial cell (specifically by AdcB or AdcC), thereby transporting the antimicrobial agent into the bacteria using the Trojan Horse strategy.

Data availability

The data supporting this article have been included as part of the ESI.† If any additional questions regarding experimental details may arise, the corresponding authors remain at the readers' disposal.

Conflicts of interest

There are no conflicts to declare.

Acknowledgements

This work was supported by the National Science Centre (UMO2017/26/A/ST5/00363 – H. K.). M. R.-Ż. is supported by 2022/47/O/ST4/01865 and A. H. is supported by NCN (UMO-2023/51/D/ST5/01798), the Polish National Agency for Academic Exchange (Grant BPN/BKK/2022/1/00005), and Excellence Initiative – Research University Grant BPIDUB.13.2024. A. D.-M. acknowledges the Research Thematic Network RED2022-134091-T financed by MCIN/AEI.

References

1 S. Lory, *The Prokaryotes – Firmicutes and Tenericutes*, 2014, vol. 4, pp. 367–370.
2 D. Ajdić, W. M. McShan, R. E. McLaughlin, G. Savić, J. Chang, M. C. Carson, C. Primeaux, R. Tian, S. Kenton, H. Jia, S. Lin, Y. Qian, S. Li, H. Zhu, F. Najar, H. Lai, J. White, B. A. Roe and J. J. Ferretti, *Proc. Natl. Acad. Sci. U. S. A.*, 2002, **99**, 14434–14439.
3 W. H. Bowen, R. A. Burne, H. Wu and H. Koo, *Trends Microbiol.*, 2018, **26**, 229–242.
4 J. A. Lemos, S. R. Palmer, L. Zeng, Z. T. Wen, J. K. Kajfasz, I. A. Freires, J. Abranches and L. J. Brady, *Microbiol. Spectrum*, 2019, **7**, 1–18.
5 S. Pant, N. J. Patel, A. Deshmukh, H. Golwala, N. Patel, A. Badheka, G. A. Hirsch and J. L. Mehta, *J. Am. Coll. Cardiol.*, 2015, **65**, 2070–2076.
6 E. Hajishengallis, Y. Parsaei, M. I. Klein and H. Koo, *Mol. Oral Microbiol.*, 2017, **32**, 24–34.
7 Y. Pan, Y. Chen, J. Chen, Q. Ma, T. Gong, S. Yu, Q. Zhang, J. Zou and Y. Li, *Mol. Oral Microbiol.*, 2021, **36**, 278–290.
8 G. Ferrazzano, T. Cantile, M. Coda, B. Alcidi, G. Sangianantoni, A. Ingenito, M. Di Stasio and M. Volpe, *Molecules*, 2016, **21**, 1008.
9 L. J. Rich and M. Seshadri, *Biomed. Opt. Express*, 2005, **6**, 3157–3162.
10 A. M. Uwitonze, N. Ojeh, J. Murererehe, A. Atfi and M. S. Razzaque, *Nutrients*, 2020, **12**, 949, DOI: **10.3390/nu12040949**.
11 J. M. Berg and Y. Shi, *Science*, 1996, **271**, 1081–1085.
12 P. Whittaker, *Am. J. Clin. Nutr.*, 1998, **68**, 442S–446S.
13 D. A. Capdevila, J. Wang and D. P. Giedroc, *J. Biol. Chem.*, 2016, **291**, 20858–20868.
14 C. Andreini and I. Bertini, *J. Inorg. Biochem.*, 2012, **111**, 150–156.
15 D. Corbett, J. Wang, S. Schuler, G. Lopez-Castejon, S. Glenn, D. Brough, P. W. Andrew, J. S. Cavet and I. S. Roberts, *Infect. Immun.*, 2012, **80**, 14–21.
16 M. I. Hood, B. L. Mortensen, J. L. Moore, Y. Zhang, T. E. Kehl-Fie, N. Sugitani, W. J. Chazin, R. M. Caprioli and E. P. Skaar, *PLoS Pathog.*, 2012, **8**, e1003068.
17 L. D. Palmer and E. P. Skaar, *Annu. Rev. Genet.*, 2016, **50**, 67–91.
18 M. T. Rahman, A. Hossain, C. H. Pin and N. A. Yahya, *Biol. Trace Elem. Res.*, 2019, **187**, 51–58.
19 R. J. Lynch, *Int. Dent. J.*, 2011, **61**, 46–54.
20 S. Shafeeq, O. P. Kuipers and T. G. Kloosterman, *Mol. Microbiol.*, 2013, **88**, 1047–1057.
21 T. Ganguly, A. M. Peterson, J. K. Kajfasz, J. Abranches and J. A. Lemos, *Mol. Oral Microbiol.*, 2021, **36**, 214–224.
22 L. Bayle, S. Chimalapati, G. Schoehn, J. Brown, T. Vernet and C. Durmort, *Mol. Microbiol.*, 2011, **82**, 904–916.
23 M. S. Akbari, K. S. Doran and L. R. Burcham, *Microorganisms*, 2022, **10**, 1501.
24 L. R. Burcham, B. Y. Le, J. N. Radin, B. L. Spencer, L. Deng, A. Hiron, M. R. Ransom, D. C. Mendonca, A. T. Belew,

N. M. El-Sayed, K. S. McIver, T. E. Kehl-Fie and K. S. Doran, *mBio*, 2020, **11**, e02302–e02320.
25 C. Y. Loo, K. Mitrakul, I. B. Voss, C. V. Hughes and N. Ganeshkumar, *J. Bacteriol.*, 2003, **185**, 2887–2900.
26 C. Y. Ong, O. Berking, M. J. Walker and A. G. McEwan, *Infect. Immun.*, 2018, **86**, e00048–e00018.
27 H. Reyes-Caballero, A. J. Guerra, E. F. Jacobsen, K. M. Kazmierczak, D. Cowart, U. M. Koppolu, R. A. Scott, M. E. Winkler and D. P. Giedroc, *J. Mol. Biol.*, 2010, **403**, 197–216.
28 T. Ganguly, A. Peterson, M. Burkholder, J. K. Kajfasz, J. Abranches and J. A. Lemos, *PLoS Pathog.*, 2022, **18**, e1010477.
29 B. Bersch, C. Bougault, L. Roux, A. Favier, T. Vernet and C. Durmort, *PLoS One*, 2013, **8**, e81168.
30 E. Loisel, L. Jacquamet, L. Serre, C. Bauvois, J. L. Ferrer, T. Vernet, A. M. Di Guilmi and C. Durmort, *J. Mol. Biol.*, 2008, **381**, 594–606.
31 B. Zheng, Q. Zhang, J. GaO, H. Han, M. Li, J. Zhang, J. Qi, J. Yan and G. F. Gao, *PLoS One*, 2011, **6**, e19510.
32 C. D. Plumptre, A. D. Ogunniyi and J. C. Paton, *Trends Microbiol.*, 2012, **20**, 485–493.
33 M. B. Brophy, J. A. Hayden and E. M. Nolan, *J. Am. Chem. Soc.*, 2012, **134**, 18089–18100.
34 T. G. Nakashige, B. Zhang, C. Krebs and E. M. Nolan, *Nat. Chem. Biol.*, 2015, **11**, 765–771.
35 J. P. Zackular, W. J. Chazin and E. P. Skaar, *J. Biol. Chem.*, 2015, **290**, 18991–18998.
36 K. Cao, N. Li, H. Wang, X. Cao, J. He, B. Zhang, Q. Y. He, G. Zhang and X. Sun, *J. Biol. Chem.*, 2018, **293**, 6075–6089.
37 A. Hecel, A. Kola, D. Valensin, H. Kozłowski and M. Rowińska-Żyrek, *Inorg. Chem.*, 2020, **59**, 1947–1958.
38 K. Garstka, D. Bellotti, J. Wątły, H. Kozłowski, M. Remelli and M. Rowińska-Żyrek, *Dalton Trans.*, 2023, **52**, 16140–16150.
39 D. Łoboda and M. Rowińska-Żyrek, *Dalton Trans.*, 2017, **46**, 13695–13703.
40 D. Łoboda and M. Rowińska-Żyrek, *Dalton Trans.*, 2018, **8**, 2646–2654.
41 K. Garstka, A. Hecel, H. Kozłowski and M. Rowińska-Żyrek, *Metallomics*, 2022, **14**, mfac042.
42 K. Garstka, G. Potoczniak, H. Kozłowski and M. Rowińska-Żyrek, *Dalton Trans.*, 2024, **53**, 2848–2858.
43 B. D. Corbin, E. H. Seeley, A. Raab, J. Feldmann, M. R. Miller, V. J. Torres, K. L. Anderson, B. M. Dattilo, P. M. Dunman, R. Gerads, R. M. Caprioli, W. Nacken, W. J. Chazin and E. P. Skaar, *Science*, 2008, **319**, 962–965.
44 S. M. Damo, T. E. Kehl-Fie, N. Sugitani, M. E. Holt, S. Rathi, W. J. Murphy, Y. Zhang, C. Betz, L. Hench, G. Fritz, E. P. Skaar and W. J. Chazin, *Proc. Natl. Acad. Sci. U. S. A.*, 2013, **110**, 3841–3846.
45 T. E. Kehl-Fie and E. P. Skaar, *Curr. Opin. Chem. Biol.*, 2010, **14**, 218–224.
46 D. Łoboda, H. Kozłowski and M. Rowińska-Żyrek, *New J. Chem.*, 2018, **42**, 7560–7568.
47 W. Aoki and M. Ueda, *Pharmaceuticals*, 2013, **21**, 1055–1081.
48 P. Gans, A. Sabatini and A. Vacca, *Talanta*, 1996, **43**, 1739–1753.
49 C. F. Baes and R. E. Mesmer, *The Hydrolysis of Cations*, Wiley, New York, 1976, p. 246.
50 A. Malakahmad, S. Tan and S. Yavari, *J. Chem.*, 2016, **1**, 1–8.
51 L. Alderighi, P. Gans, A. Ienco, D. Peters, A. Sabatini and A. Vacca, *Coord. Chem. Rev.*, 1999, **184**, 311–318.
52 *Origin(Pro), Version 2016*.
53 W. Bal, J. Lukszo, M. Jeżowska-Bojczuk and K. S. Kasprzak, *Chem. Res. Toxicol.*, 1995, **8**, 683–692.
54 J. M. Mouillon, S. K. Eriksson and P. Harryson, *Plant Physiol.*, 2008, **148**, 1925–1937.
55 H. Irving and R. J. P. Williams, *J. Chem. Soc.*, 1953, 3192–3210.
56 H. Irving and R. J. P. Williams, *Nature*, 1948, **162**, 746–747.
57 T. Sierpińska, K. Orywal, J. Kuc, M. Golebiewska and M. Szmitkowski, *Int. J. Prosthodontics*, 2013, **26**, 423–428.
58 R. Fors and M. Persson, *Eur. J. Orthod.*, 2006, **28**, 292–297.
59 B. Xu, L. Wang, C. Yang, R. Yan, P. Zhang, M. Jin, H. Du and Y. Wang, *J. Adv. Res.*, 2025, **67**, 301–315.